Mineralogy and Petrology (1988) 38: 201 – 211

Mineralogy
and
Petrology

Sigloite: The Oxidation Mechanism in $[M_2^{3+}(PO_4)_2(OH)_2(H_2O)_2]^{2-}$ Structures

F. C. Hawthorne

Department of Geological Sciences, University of Manitoba, Winnipeg, Manitoba, Canada

With 3 Figures

Received May 15, 1987;
accepted February 18, 1988

Summary

The crystal structure of sigloite, $Fe^{3+}[(H_2O)_3OH]\,[Al_2(PO_4)_2(OH)_2(H_2O)_2]\cdot 2\,H_2O$, triclinic, a 5.190(2), b 10.419(4), c 7.033(3) Å, α 105.00(3), β 111.31(3), γ 70.87(3)°, V 330.5(2) $Å^3$, $Z = 1$, space group $P\bar{1}$, has been refined to an R index of 5.3% using 1713 observed ($I > 2.5\,\sigma I$) reflections collected with graphite-monochromated MoKα X-rays. Sigloite is isostructural with the laueite-group minerals. Corner-linked $[Al\phi_5]$ chains (ϕ: unspecified ligand) are cross-linked by (PO_4) tetrahedra to form a mixed corner-linked tetrahedral-octahedral sheet of composition $[Al_2(PO_4)_2(OH)_2(H_2O)_2]^{2-}$. These sheets are linked by $(Fe^{3+}O_2(OH, H_2O)_4)$ octahedra and two (H_2O) groups that participate in a hydrogen-bonding network. Sigloite is the oxidized equivalent of paravauxite, $Fe^{2+}(H_2O)_4[Al_2(PO_4)_2(OH)_2(H_2O)_2]\cdot 2\,H_2O$, and detailed comparison of the two structures shows that the oxidation mechanism involves loss of hydrogen from one of the (H_2O) groups coordinating the Fe^{3+}, and positional disorder of both the Fe^{3+} and (OH) and (H_2O) ligands.

Zusammenfassung

Sigloit: Der Oxidationsmechanismus in $[M_2^{3+}(PO_4)_2(OH)_2(H_2O)_2]^{2-}$ Strukturen

Die Kristallstruktur von Sigloit, $Fe^{3+}[(H_2O)_3OH]\,[Al_2(PO_4)_2(OH)_2(H_2O)_2]\cdot 2\,H_2O$, triklin, a 5,190(2), b 10,419(4), c 7,033(3) Å, α 105,00(3), β 111,31(3), γ 70,87(3)°, V 330,5(2) $Å^3$, $Z = 1$, Raumgruppe $P\bar{1}$, wurde für 1713 beobachtete Reflexe ($I > 2{,}5\,\sigma I$), die mit MoKα-Röntgenstrahlung (Graphit-Monochromator) gesammelt wurden, auf einen R-Wert von 5,3% verfeinert. Sigloit ist isotyp mit den Mineralen der Laueit-Gruppe. Über Ecken verknüpfte $[Al\phi_5]$-Ketten (ϕ: nicht spezifizierter Ligand) werden über (PO_4)-Tetraeder zu ebenfalls über Ecken verknüpfte Tetraeder-Oktaeder-Schichten der Zusammensetzung $[Al_2(PO_4)_2(OH)_2(H_2O)_2]^{2-}$ verbunden. Diese Schichten werden über $(Fe^{3+}O_2(OH, H_2O)_4)$-Oktaeder und zwei (H_2O)-Gruppen, die am

Wasserstoffbrücken-Netzwerk beteiligt sind, verbunden. Sigloit ist das oxidierte Analogon zu Paravauxit, $Fe^{2+}(H_2O)_4[Al_2(PO_4)_2(OH)_2(H_2O)_2] \cdot 2H_2O$; ein detaillierter Vergleich dieser beiden Strukturen zeigt, daß der Oxidationsmechanismus sowohl den Verlust eines Wasserstoffatoms (H_2O)-Gruppe, welche ein Fe^{3+}-Atom koordiniert, als auch eine Fehlordnung der Punktlagen von Fe^{3+} und von den (OH) und (H_2O)-Liganden bedingt.

Introduction

Sigloite, $(Fe^{3+},Fe^{2+})Al_2(PO_4)_2(OH)_2(H_2O,OH)_8$, is a pegmatite phosphate mineral reported by *Hurlbut* and *Honea* (1962) from the Siglo XX Mine, Llallagua, Bolivia. It is found, associated with paravauxite, wavellite, metavauxite, crandallite and childrenite, in open fractures cutting cassiterite veins. Sigloite is an oxidation pseudomorph after paravauxite, and presumably belongs to a supergene stage postdating the final phase of hydrothermal mineralization that resulted in the other phosphate minerals (*Hurlbut* and *Honea,* 1962).

Experimental Methods

The material used in this work is from the Siglo XX Mine, and has been deposited at the Department of Mineralogy and Geology, Royal Ontario Museum, Toronto, collection number M42149. The crystal used for the data collection was of tabular form on {010}. It was mounted on a Nicolet R3m automated four-circle diffractometer, and the cell dimensions were refined from the setting angles of twenty-five automatically aligned intense reflections; these are listed in Table 1, together with other information pertinent to data collection and refinement. Intensity data were collected according to the experimental procedure of *Hawthorne* (1985). A

Table 1. *Cell and Data Collection Information for Sigloite*

a = 5.190(2)Å	Crystal size(mm) =	0.06x0.18x0.24
b = 10.419(4)	Rad/Mono	MoKα/Graphite
c = 7.033(3)	Total Unique $\|F_o\|$	1943
α = 105.00(3)°	No. of $\|F_o\|$ ($I>2.5\sigma I$)	1713
β = 111.31(3)	R (observed)	5.3%
γ = 70.87(3)	R_w (observed)	5.9%
V = 330.5(2)Å^3		

Space Group: $P\bar{1}$

Unit cell contents: $Fe^{3+}(H_2O,OH)_4[Al_2(PO_4)_2(OH)_2(H_2O)_2].2H_2O$

$R = \Sigma(|F_o|-|F_c|)/\Sigma|F_o|$

$R_w = [\Sigma w(|F_o|-|F_c|)^2/\Sigma wF_o^2]^{1/2}$, w = 1

Temperature factor form used: $\exp(-2\pi^2[h^2a^{*2}U_{11}+....2hka^*b^*U_{12}+...])$

total of 1943 reflections was collected out to a maximum 2θ of 60°. An empirical absorption correction was applied (ψ-scan method, flat-plate calculation), reducing *R* (symmetric) for the azimuthal data from 6.4% to 3.3%. Lorentz, polarization and background corrections were done, and the data were reduced to structure factors; of the 1943 unique reflections, 1713 were classed as observed ($I > 2.5\sigma(I)$).

Refinement

Scattering curves for neutral atoms together with anomalous dispersion coefficients were taken from *Cromer* and *Mann* (1968) and *Cromer* and *Liberman* (1970). *R* indices are of the form given in Table 1, and are expressed as percentages.

Table 2. *Positional and Isotropic Thermal Parameters for Sigloite*

	x	y	z	$U^*_{equiv.}$
Fe	0.0185(5)	0.0012(3)	-0.0066(4)	1.95(3)
Al(1)	0	1/2	0	0.98(5)
Al(2)	0	1/2	1/2	1.09(5)
P	0.3311(2)	0.6693(1)	0.9107(1)	0.98(3)
O(1)	0.1692(6)	0.6438(3)	0.0357(4)	1.4(1)
O(2)	0.2883(6)	0.5796(3)	0.6971(4)	1.4(1)
O(3)	0.2191(7)	0.8229(3)	0.8842(5)	1.9(1)
O(4)	0.3464(6)	0.3607(3)	0.9692(4)	1.4(1)
O(5)	0.1374(6)	0.5028(3)	0.2899(4)	1.3(1)
O(6)	0.2518(7)	0.3188(3)	0.5546(5)	1.8(1)
O(7A)	0.2917(15)	0.9843(7)	0.2912(11)	2.7(1)
O(7B)	0.3622(15)	0.0105(8)	0.2388(11)	2.7(1)
O(8A)	0.2306(16)	0.0959(7)	-0.0641(11)	2.6(1)
O(8B)	0.1277(16)	0.1005(7)	0.8381(11)	2.6(1)
O(9A)	0.2185(15)	0.8120(7)	0.4837(11)	2.5(1)
O(9B)	0.3071(15)	0.8638(7)	0.5538(11)	2.5(1)
H(6)A	0.410(11)	0.276(5)	0.530(8)	1.0**
H(6)B	0.294(11)	0.321(5)	0.659(9)	1.0**

$^*U_{equiv} = (U_{11}U_{22}U_{33})^{1/3}\times10^4$; **Fixed during refinement

Table 3. *Anisotropic Temperature Factor Coefficients for Sigloite*

	$^*U'_{11}$	U'_{22}	U'_{33}	U'_{12}	U'_{13}	U'_{23}
Al(1)	104(7)	174(8)	61(6)	-80(6)	27(5)	32(5)
Al(2)	110(7)	197(8)	57(6)	-73(6)	25(5)	37(6)
P	92(4)	156(4)	80(4)	-59(3)	28(3)	39(3)
O(1)	150(12)	212(14)	108(12)	-103(11)	61(10)	28(10)
O(2)	125(12)	240(14)	91(11)	-98(11)	37(9)	36(10)
O(3)	233(15)	192(14)	213(15)	-54(12)	102(12)	93(11)
O(4)	101(11)	238(14)	96(12)	-77(10)	30(9)	32(10)
O(5)	111(12)	249(14)	72(11)	-82(11)	32(9)	51(10)
O(6)	173(14)	252(15)	112(13)	-49(12)	43(11)	58(11)

$^*U'_{ij} = U_{ij}\times10^4$

Table 4. *Selected Bond Lengths (Å) in Sigloite*

P-O(1)a	1.533(4)		Fe-O(3)f	1.924(4)
P-O(2)	1.532(3)		Fe-O(3)e	2.024(4)
P-O(3)	1.549(3)		Fe-O(7A)g	2.073(7)
P-O(4)b	1.543(3)		Fe-O(7A)d	2.068(7)
<P-O>	1.539		Fe-O(8A)	1.895(11)
			Fe-O(8A)h	2.127(11)
Al(1)-O(1)	1.894(4)	x2	<Fe-O(A)>	2.019
Al(1)-O(4)c	1.948(3)	x2		
Al(1)-O(5)	1.895(4)	x2	Fe-O(3)f	1.924(4)
<Al(1)-O>	1.912		Fe-O(3)e	2.024(4)
			Fe-O(7B)	1.990(7)
Al(2)-O(2)	1.886(3)	x2	Fe-O(7B)h	2.072(7)
Al(2)-O(5)	1.869(3)	x2	Fe-O(8B)c	2.001(11)
Al(2)-O(6)	1.953(3)	x2	Fe-O(8B)i	2.221(11)
<Al(2)-O>	1.903		<Fe-O(B)>	2.039
O(6)-H(6)A	0.85(6)		H(6)A-O(9A)j	1.87(5)
O(6)-H(6)B	0.68(6)		H(6)A-O(9B)j	1.85(5)
H(6)A-H(6)B	1.19(9)		H(6)B-O(4)	2.04(6)
O(6)-O(9A)j	2.716(8)		O(6)-H(6)A-O(9A)j	172(5)°
O(6)-O(9B)j	2.665(8)		O(6)-H(6)A-O(9B)j	160(6)
O(6)-O(4)	2.715(4)		O(6)-H(6)B-O(4)	168(5)

a: x,y,1+z; b: 1-x,1-y,2-z; c: x,y,z-1; d: $\bar{x}$,1-y,$\bar{z}$; e: $\bar{x}$,1-y,1-z; f: x,y-1,z-1; g: x,y-1,z; h: $\bar{x}$,$\bar{y}$,$\bar{z}$,; i: $\bar{x}$,$\bar{y}$,1-z; j: 1-z,1-y,1-z.

The coordinates of paravauxite (*Baur,* 1969) were used as starting parameters, and the refinement converged at an R index of 14.8% for an isotropic thermal model. The isotropic temperature factors for some of the atoms were up to an order of magnitude larger than others. This was not unexpected, as all the aberrant atoms were associated with the $(\mathrm{Fe}\phi_6)$ group that had undergone partial oxidation/dehydroxylation. Fourier maps calculated at this stage showed the density around these positions to be very elongate or even bimodal; consequently the atoms on general positions were split into "half-atoms", the positions of the "half-atoms" were allowed to vary freely, but the isotropic temperature factors of each of the pair of "half-atoms" were constrained to be equal. This model converged at an R index of 8.8%, and the values of the "half-atom" isotropic temperature factors were much more reasonable. The separations of the "half-atoms" ranged up to 0.8 Å, the aberrant temperature factors being due to gross positional disorder of the atoms involved. Conversion to anisotropic temperature factors and least-squares refinement of all variable resulted in convergence at an R index of 5.5%. The Fe atom was exaggeratedly anisotropic at this stage, and as it is bonded to four oxygens, it seemed reasonable to assume that it also has some positional disorder about its ideal position; Fourier maps also confirmed the anisotropic distribution of density about the origin. At this stage, the hydrogen atoms were visible around the (non-disordered) O (6) (H_2O) group on difference Fourier maps. Insertion of the hydrogen positions, disorder of Fe off the origin and least-squares refinement of all variables converged to an R index of 5.3%.

Final parameters are given in Tables 2 and 3, selected interatomic distances in Tables 4 and 5, and a bond-valence calculation in Table 6. Observed and calculated structure-factors are available from the author.

Table 5. *Polyhedral Edge-lengths (Å) and Angles (°) in Sigloite*

0(1)a-0(2)	2.544(4)	0(1)a-P-0(2)	112.2(2)
0(1)a-0(3)	2.496(5)	0(1)a-P-0(3)	108.1(2)
0(1)a-0(4)b	2.512(5)	0(1)a-P-0(4)b	109.5(2)
0(2)-0(3)	2.511(4)	0(2)-P-0(3)	109.2(2)
0(2)-0(4)b	2.505(3)	0(2)-P-0(4)b	109.1(2)
0(3)-0(4)b	2.512(4)	0(3)-P-0(4)b	108.7(2)
<0-0>P	2.513	<0-P-0>	109.5
0(1)-(4)c	2.755(4) x2	0(1)-Al(1)-0(4)c	91.6(1) x2
0(1)-0(4)e	2.679(5) x2	0(1)-Al(1)-0(4)e	88.4(1) x2
0(1)-0(5)	2.668(5) x4	0(1)-Al(1)-0(5)	89.5(1) x4
0(1)-0(5)d	2.691(4) x4	0(1)-Al(1)-0(5)d	90.5(1) x4
<0-0>Al(1)	2.692	<0-Al(1)-0>	90.0
0(2)-0(4)	2.655(4) x2	0(2)-Al(2)-0(5)	90.0(1) x2
0(2)-0(5)e	2.656(5) x2	0(2)-Al(2)-0(5e)	90.0(1) x2
0(2)-0(6)	2.686(5) x2	0(2)-Al(2)-0(6)	88.1(1) x2
0(2)-0(6)e	2.744(4) x2	0(2)-Al(2)-0(6e)	91.2(1) x2
0(5)-0(6)	2.791(5) x2	0(5)-Al(2)-0(6)	93.8(1) x2
0(5)-0(6)e	2.612(4) x2	0(5)-Al(2)-0(6e)	86.2(1) x2
<0-0>Al(2)	2.691	<0-Al(2)-0>	90.0
0(3)f-0(7A)g	2.882(7)	0(3)f-Fe-0(7A)g	92.2(2)
0(3)f-0(7A)d	2.828(7)	0(3)f-Fe-0(7A)d	90.2(2)
0(3)f-0(8A)	2.791(9)	0(3)f-Fe-0(8A)	93.9(3)
0(3)f-0(8A)h	2.839(10)	0(3)f-Fe-0(8A)h	88.8(3)
0(3)e-0(7A)g	2.828(7)	0(3)e-Fe-0(7A)g	87.3(2)
0(3)e-0(7A)d	2.882(7)	0(3)e-Fe-0(7A)d	89.5(2)
0(3)e-0(8A)	2.839(10)	0(3)e-Fe-0(8A)	92.8(3)
0(3)e-0(8A)h	2.790(9)	0(3)e-Fe-0(8A)h	84.4(2)
0(7A)g-0(8A)	2.895(11)	0(7A)g-Fe-0(8A)	93.6(4)
0(7A)g-0(8A)h	2.871(11)	0(7A)g-Fe-0(8A)h	86.2(4)
0(7A)d-0(8A)	2.871(11)	0(7A)d-Fe-0(8A)	92.8(4)
0(7A)d-0(8A)h	2.895(11)	0(7A)d-Fe-0(8A)h	87.3(3)
<0-0>A:Fe	2.851	<0-Fe-0>A	89.9
0(3)f-0(7B)	2.771(7)	0(3)f-Fe-0(7B)	90.1(2)
0(3)f-0(7B)h	2.883(7)	0(3)f-Fe-0(7B)h	92.3(2)
0(3)f-0(8B)c	2.858(9)	0(3)f-Fe-0(8B)c	93.5(3)
0(3)f-0(8B)i	2.915(10)	0(3)f-Fe-0(8B)i	89.1(2)
0(3)e-0(7B)	2.883(7)	0(3)e-Fe-0(7B)	91.8(2)
0(3)e-0(7B)h	2.770(7)	0(3)e-Fe-0(7B)h	85.1(2)
0(3)e-0(8B)c	2.915(10)	0(3)e-Fe-0(8B)c	92.8(3)
0(3)e-0(8B)i	2.858(9)	0(3)e-Fe-0(8B)i	84.5(2)
0(7B)-0(8B)c	2.903(11)	0(7B)-Fe-0(8B)c	93.4(4)
0(7B)-0(8B)i	2.950(13)	0(7B)-Fe-0(8B)i	88.8(4)
0(7B)h-0(8B)c	2.950(13)	0(7B)h-Fe-0(8B)c	92.8(4)
0(7B)h-0(8B)i	2.903(11)	0(7B)h-Fe-0(8B)i	85.0(3)
<0-0>B:Fe	2.880	<0-Fe-0>B	89.9

Description of the Structure

Discounting the positional disorder at several of the atomic positions, the sigloite structure is isostructural with the paravauxite (*Baur*, 1969) and laueite (*Moore*, 1965) structures. Corner-sharing $[M^{3+}\phi_5]$ chains (ϕ: unspecified ligand) extend parallel to the Z-axis and are further linked along their lengths by (PO_4) tetrahedra to form $[Al(PO_4)\phi_2]$ chains (*Moore*, 1970). The O(5) oxygen that bridges along the length of this chain is an (OH) anion, as shown by the local bond-valence sum (Table 6); as it is bonded to two Al^{3+} cations, O(5) will only be a weak (at best) hydrogen-bond donor. The (PO_4) tetrahedral vertices not linked to the central octahedral chain cross-link to adjacent chains to form a mixed tetrahedral-octahedral sheet (Fig. 1) of composition $[Al_2(PO_4)_2(OH)_2(H_2O)_2]$. These sheets are

Table 6. *Bond-Valence Table for Sigloite, Calculated with the Curves of Brown (1981).* Anions O(7 A), O(7 B), O(8 A), O(8 B), O(9 A) and O(9 B) are omitted; these form the ten different hydrogen-bonding arrangements shown in Fig. 3

	P	Al(1)	Al(2)	Fe	H(6)A	H(6)B	$\sum$
O(1)	1.274	0.514					1.788 (+H)*
O(2)	1.277		0.524				1.801 (+H)*
O(3)	1.218			0.642^{+} 0.481^{+}			1.860^{+} 1.699^{+}
O(4)	1.239	0.456				0.23	1.925
O(5)		0.513	0.544				1.057 (=OH)
O(6)			0.451		0.77	0.77	1.991
$\sum$	5.008	2.966	3.038	(3.030)** (2.870)**	—	1.00	

* Indicates a further hydrogen-bonding contribution from configurations involving O(8 A) and O(8 B) (see Fig. 3) for O(1), and from O(5) (=OH) for O(2).

** Bond-valence sums include contributions to O(7 A), O(7 B), O(8 A) and O(8 B).

$^{+}$ Indicates alternate configurations.

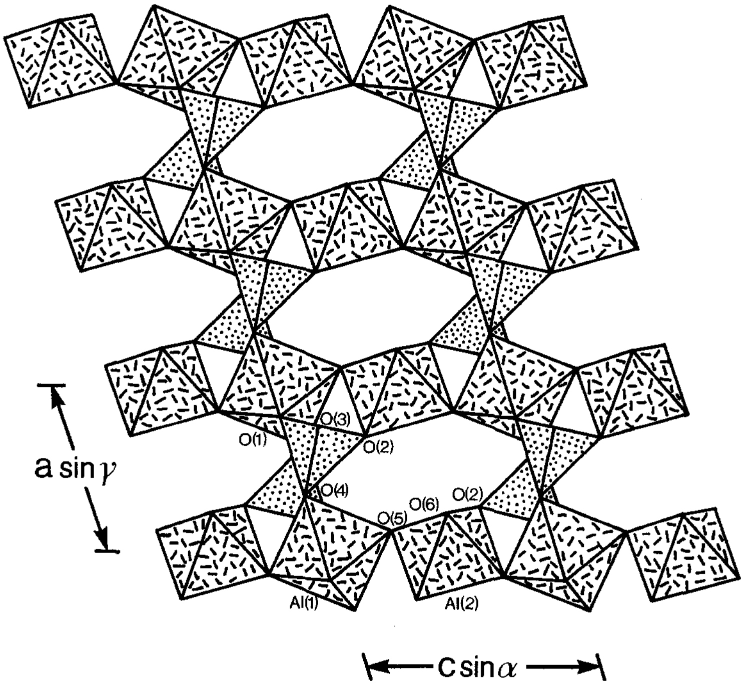

Fig. 1. The heteropolyhedral $[Al_2(PO_4)_2(OH)_2(H_2O)_2]^{2+}$ sheet in sigloite, projected down in the Y axis

parallel to (010), and are cross-linked by $(M\phi_6)$ octahedra (Fig. 2) which share one oxygen with each sheet on either side, and have four anions that hydrogen bond to the adjacent sheets. In addition, there is an (H_2O) group that is not bonded to any cation but is held in place by a network of hydrogen bonds (*Baur,* 1969).

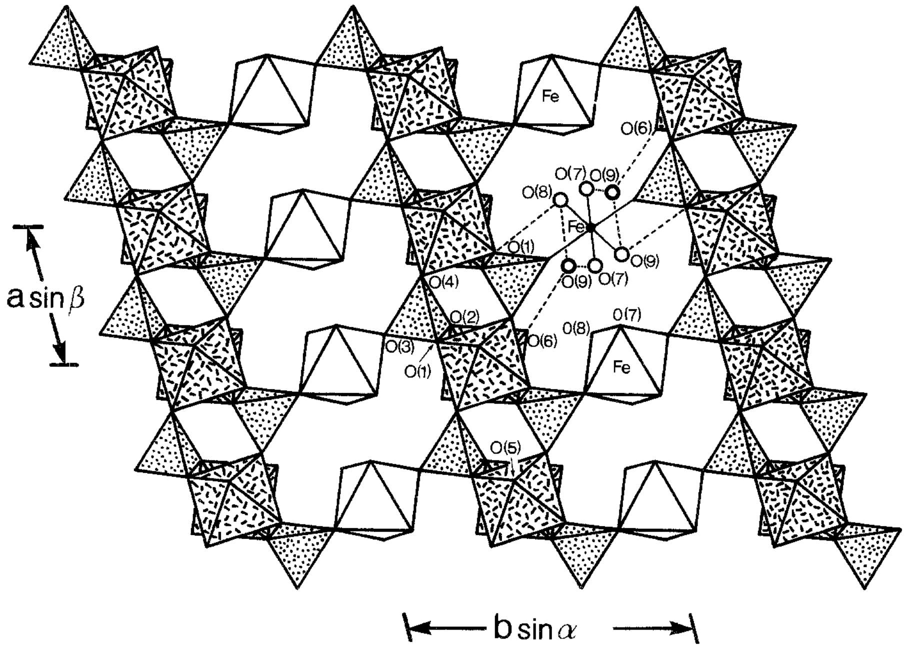

Fig. 2. The cross-linkage of the heteropolyhedral sheets by $[Fe^{3+}(H_2O, OH)_6]$ octahedra in sigloite

The Oxidation Mechanism in Sigloite

Detailed comparison of the bond lengths in sigloite and paravauxite shows that the P—O and Al—O bond lengths in both structures do not differ by more than two standard deviations, and thus the tetrahedral-octahedral sheet seems to be relatively unaffected by oxidation. Conversely, the linking octahedron is much smaller in sigloite, reflecting its occupancy by Fe^{3+} rather than by Fe^{2+} as in paravauxite. However, this is not the only change to take place upon oxidation; such an increase in charge must be compensated elsewhere by a loss of charge so that the overall crystal remains neutral. This is most easily accomplished by a loss of hydrogen from one of the (H_2O) groups in the structure. Although this hydrogen loss could occur at any (H_2O) group in the structure, the similarity of the sheet modules in both paravauxite and sigloite indicates that the module (H_2O) groups are unaffected. Consequently the hydrogen must be lost from one of the (H_2O) groups bonded to the sheet-bridging cation. This is advantageous both with regard to the actual oxidation mechanism, and with regard to the local bond-valence requirements. Oxidation can occur most easily by the reaction ...

$$Fe^{2+} + H_2O = Fe^{3+} + (OH)^- + H^+ \rightarrow$$

... with the corresponding loss of a proton. Consequently one of the (H_2O) groups bonded to each Fe^{3+} becomes an (OH) group, and there must be considerable local rearrangement in order for the local bond-valence requirements of all the ligand oxygens to be satisfied.

Examination of Tables 2 and 4 shows that around the disordered Fe^{3+} position, all the oxygens were split into "half-atoms" except for the two (*trans*) oxygens belonging to phosphate groups, which were quite well-behaved. Specific local configurations around Fe were identified by considering the possible octahedral edge-lengths and angles from the large number of values calculated from the disordered configurations. Configurations with excessive values of (O—O) edge-lengths and (O—Fe—O) angles were discarded to leave the values given in Table 5, which should represent the local configurations. Projection of the octahedral configurations on to a plane perpendicular to the O (3)—O (3) axis of the octahedra shows that the A and B configurations are essentially rotated relative to each other; this presumably arises from different hydrogen-bonding schemes that must arise around the $(\mathrm{Fe}\phi_6)$ octahedra accompanying oxidation of the central cation from divalent to trivalent state.

The hydrogen-bonding scheme in the unoxidized state is given by Baur (1969). In sigloite, some aspects of the hydrogen-bonding scheme remain unchanged: the hydroxyl ion O (5) is a weak hydrogen-bond donor to O (2), and O (6) is a hydrogen-bond donor to O (4); the other hydrogen atom attached to O (6) still hydrogen-bonds to the O (9) (H_2O) group, but in sigloite, O (9) is split into two positions, both of which still act as hydrogen-bond acceptors to O (6). The hydrogen-bond arrangements around O (7) and O (8) in sigloite are complicated both by the splitting of these oxygens and by the fact that the Fe^{3+} cation is disordered off its ideal central position. These two factors combine to give four different environments for both the O (7) and O (8) atoms: each is split into A and B configurations, and then each A and B configuration is split into two by whether or not the Fe^{3+} cation is displaced towards or away from the oxygen. These configurations are summarised in Fig. 3.

Consider first the A configuration involving O (7 A) and O (8 A). The Fe—O (8 A) bond-valence is 0.70 v.u. (Table 5), suggesting that the hydrogen is lost predominantly from O (8 A) in the A octahedral configuration. Assuming essentially no hydrogen-bonding between the remaining hydrogen and any other anions, this still only gives a bond-valence sum of 1.70 v.u. at O (8 A). This suggests additional hydrogen-bonding between O (9 A) and/or O (9 B) and O (8 A) to bring the bond-valence sum at O (8 A) up to the ideal value of 2.0 v.u. (Fig. 3 c). The Fe′—O (8 A) bond-valence is 0.36 v.u. (Fig. 3 d), suggesting that the O (8 A) in this configuration does not lose a hydrogen atom and remains a (H_2O) group; note that this is in accord with the necessary charge compensation to allow the crystal to remain neutral. The O (8 A) in this configuration hydrogen-bonds to O (1) and O (9 A) and/or O (9 B) (Fig. 3 d). Loss of hydrogen solely at O (8 A) for the A configuration means that O (7 A) remains a (H_2O) group. In line with this, the bond-valences of the bonds between the two disordered Fe^{3+} positions and O (7 A) are approximately equal at 0.420 and 0.425 v.u. respectively, hydrogen bonding to both split O (9 A) and O (9 B) atoms in one case, but only O (9 B) in the other case (Figs. 3 a, b).

Consider next the B configuration involving O (7 B) and O (8 B). The distribution of observed bond-valences in this case (Table 6) suggests that the hydrogen atom is lost equally at O (7 B) and O (8 B), in the configurations involving bond-valences of 0.53 and 0.51 v.u. for O (7 B) and O (8 B), respectively. When O (7 B) = OH (Fig. 3 e), there is a short strong hydrogen-bond from O (9 B) to O (7 B), with O (9 B)—O (7 B) = 2.335 (11) Å, and the remaining hydrogen atom on O (7 B) is not significantly involved in the hydrogen-bonding. Conversely, when O (7 B) = H_2O, there are weaker hydrogen bonds from O (7 B) to O (9 B); as shown in Fig. 3 f, these split

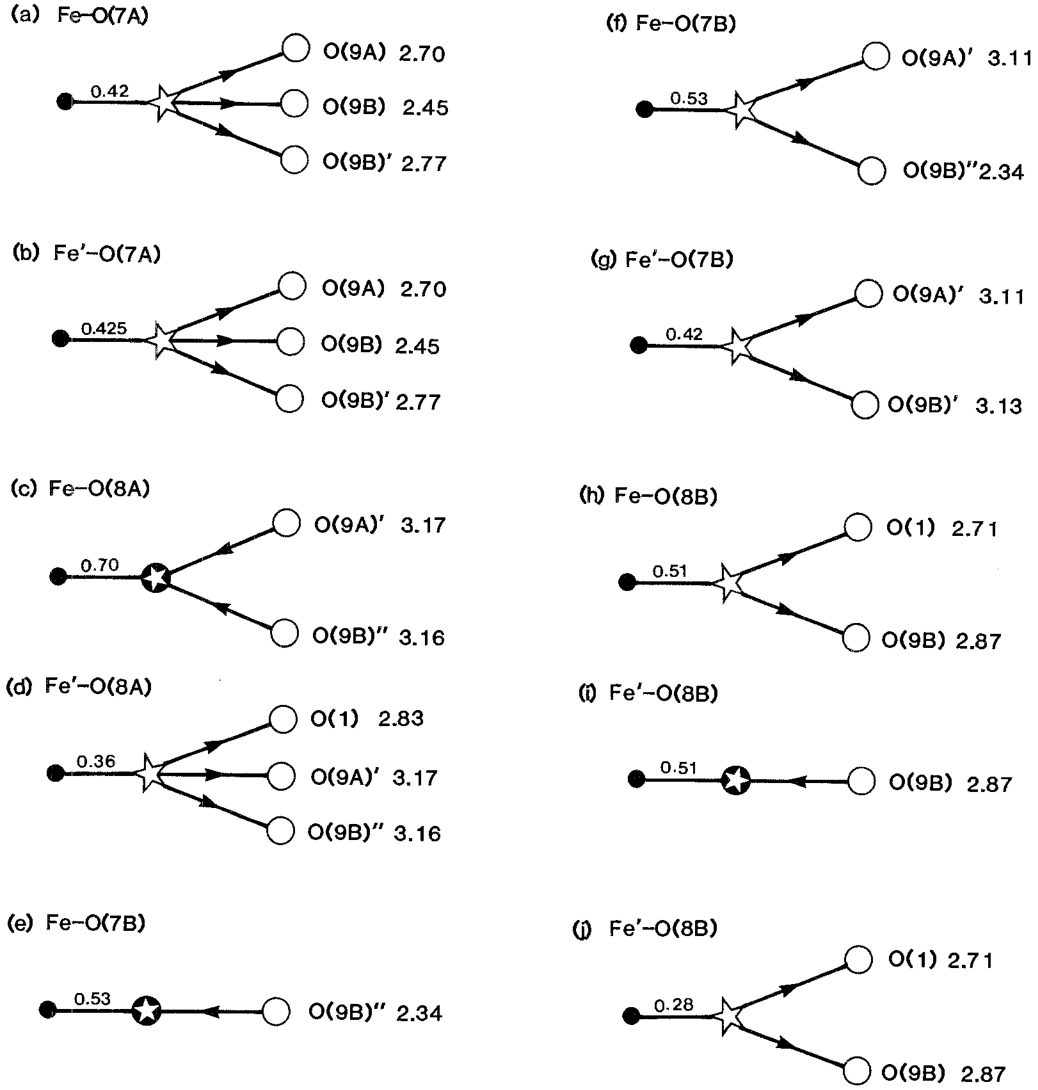

Fig. 3. Diagrammatic representation of the local hydrogen-bond configurations about the $[Fe^{3+}(H_2O, H)_6]$ octahedra in sigloite: ● = Fe; ✪= OH; ☆= H_2O; distances are in Å; the arrows indicate the direction of the hydrogen-bonding (donor→-acceptor); the parentheses indicate that *either* one *or* the other of the bonds bracketed occurs

O (9) groups are not adjacent to each other, and therefore must involve coupling of neighbouring configurations. The configuration in which the Fe—O (7 B) bond has a bond-valence of 0.42 v.u. is shown in Fig. 3 g; O (7 B) is predominently (H_2O) in this configuration, and hydrogen-bonds to O (9 A) and O (9 B), again involving coupling between adjacent O (9) configurations. The configurations where Fe—O (8 B) = 0.51 v.u. are shown in Figs. 3 h, i for O (8 B) = H_2O and OH, respectively. When O (8 B) = H_2O, there are hydrogen-bonds to O (1) and O (9 B); when O (8 B) = OH, there is strong hydrogen-bonding from O (9 B) to O (8 B), and no hydrogen-bonding between O (8 B) and O (1). When the Fe—O (8 B) bond-valence is 0.28 v.u. (Fig. 3 j), O (8 B) = H_2O and hydrogen-bonds to O (1) and O (9 B).

As indicated above, there is significant coupling between adjacent configurations. However, all schemes suggested in Fig. 3 lead to approximate local satisfaction of bond-valence requirements about all of the split-atom positions in sigloite. It remains to be shown that the bond-valence requirements about the remaining anions O(1)→O(6) are also satisfied; as is apparent from Table 5, O(1) and O(3) need significant additional bond-valence contribution.

Consider first the O(1) anion. There are two close contacts that can involve hydrogen-bonding: O(1)—O(8 B) = 2.709(7) Å and O(1)—O(8 A) = 2.843(7) Å. With regard to O(8 A), this will contribute a hydrogen-bond for about one-quarter of the total configurations (i.e. when the O(8 A) position is occupied by H_2O); with regard to O(8 B), this will contribute a hydrogen-bond for about seven-sixteenths of the total configurations (i.e. when O(8 B) = H_2O). Thus O(1) receives a hydrogen-bond from one of the split O(8) positions for about three-quarters of the total configurations. For the O(3) anion, this receives a hydrogen-bond from either O(9 A) or O(9 B) for any one configuration, and receives a hydrogen-bond from O(8 A) when O(8 A) = H_2O (i.e. about one-quarter of the configurations); possibly there is coupling between O(8 A) and O(9 A) in this configuration, as O(3)—O(9 A) is significantly longer (2.788(9) Å) than O(3)—O(9 B) which is 2.683(10) Å. Thus both O(1) and O(3) receive their required bond-valence contributions from the hydrogen-bond schemes proposed.

Conclusions

Sigloite is the oxidized equivalent of paravauxite. The heteropolyhedral sheet modules are virtually identical in each structure, and the changes accompanying oxidation of the intrasheet $Fe^{2+} \rightarrow Fe^{3+}$ are localized between the sheets. Local geometry and bond-valence arguments have been used to propose a series of hydrogen-bond configurations that must occur in the crystal to give rise to the observed average arrangement; it is shown that this oxidation proceeds with conservation of local bond-valence requirements.

Acknowledgements

This work was funded by the Natural Sciences and Engineering Council of Canada, in the form of a fellowship, an operating grant and major equipment grant to F. C. H.

References

Baur WH (1969) The crystal structure of paravauxite, $Fe^{2+}Al_2(PO_4)_2(OH)_2(OH_2)_6 \cdot 2H_2O$. Neues Jahrb Miner Monatsh 1969: 430–433

Brown ID (1981) The bond-valence method: an empirical approach to chemical structure and bonding. In: *O'Keeffe M, Navrotsky A* (eds) Structure and bonding in crystals, II. Academic Press, New York

Cromer DT, Liberman D (1970) Relativistic calculation of anomalous scattering factors for X-rays. J Chem Phys 53: 1891–1898

— *Mann JB* (1968) X-ray scattering factors computed from numerical Hartree-Fock wave functions. Acta Cryst A 24: 321–324

Hawthorne FC (1985) Refinement of the crystal structure of bloedite: structural similarities in the $\{(VI)M[(IV)T\varnothing_4]_2\varnothing n\}$ finite-cluster minerals. Can Min 23: 669–674

Hurlbut CS, Honea R (1962) Sigloite, a new mineral from Llallagua, Bolivia. Am Min 47: 1–8

Moore PB (1965) The crystal structure of laueite. Am Min 50: 1884–1892

— (1970) Structural hierarchies among minerals containing octahedrally coordination oxygen. I. Stereoisomerism among corner-sharing octahedral and tetrahedral chains. Neues Jahrb Miner Monatsh 1970: 163–173

Author's address: Dr. *Frank C. Hawthorne,* Department of Geological Sciences, University of Manitoba, Winnipeg, Manitoba, Canada, R3T 2N2.